Rakenteiden Mekaniikka (Journal of Structural Mechanics)
Vol. 48, No 4, 2015, pp. 199 – 210
rmseura.tkk.fi/rmlehti/

VERTAISARVIOITU
KOLLEGIALT GRANSKAD
PEER-REVIEWED
www.tsv.fi/tunnus

Some aspects on efficient solution of creep problems

Reijo Kouhia[1], Pekka Marjamäki, and Jorma Kivilahti

Summary. Integration of inelastic constitutive models by implicit schemes, require local Newton's iteration to solve the discretized non-linear evolution equations at the integration point level. Choise of the starting values in the Newton's iteration affects on the success of the iteration at the local integration point level. This note describes a simple modification on the approach proposed by Schreyer giving increased robustness on the local iteration process. Also the effect of line search and quasi-Newton methods in the solution of the global equilibrium iterations is investigated.

Key words: creep, implicit integration, initial values, Newton's method

Received 15 December 2015. Accepted 31 December 2015. Published online 8 January 2016.

Introduction

Implicit schemes are often used in the temporal integration of constitutive equations [3, 7, 8, 10, 11, 18, 19]. Success in such methods depends primarily on two factors: firstly how the small local non-linear system at the integration point level is solved and secondly, is the Jacobian matrix of the discretized constitutive model (i.e. the algorithmic tangent stiffness) properly formulated and evaluated. If the material Jacobian matrix is properly evaluated, asymptotically quadratic convergence of the global equilibrium iterations can be achieved. Convergence of the global equilibrium equations is a primary factor affecting to the cost of the computation. Since the Newton's method is only locally convergent, the global equilibrium iterations might diverge or it can take quite a many iterations before the domain of attraction is reached and the process starts to converge quadratically. As it will be shown, a line search procedure can save a considerable amount of computing time when large time steps are used.

Inelastic material model and its numerical integration

In this study the assumption of small strains is adopted, and therefore the rate of strain can be additively decomposed in elastic $\dot{\boldsymbol{\epsilon}}^{\mathrm{e}}$, thermal $\dot{\boldsymbol{\epsilon}}^{\mathrm{th}}$ and inelastic $\dot{\boldsymbol{\epsilon}}^{\mathrm{in}}$ components

$$\dot{\boldsymbol{\epsilon}} = \dot{\boldsymbol{\epsilon}}^{\mathrm{e}} + \dot{\boldsymbol{\epsilon}}^{\mathrm{th}} + \dot{\boldsymbol{\epsilon}}^{\mathrm{in}}. \tag{1}$$

[1]Corresponding author. reijo.kouhia@tut.fi

Assuming the inelastic strain to be strictly deviatoric, the evolution equation for the inelastic strain rate suitable for modeling secondary creep can be written as

$$\dot{\boldsymbol{\epsilon}}^{\text{in}} = \tfrac{3}{2} f \exp\left(\frac{-Q}{R\theta}\right) \sinh^m\left(\frac{\bar{\tau}}{Y}\right) \frac{\boldsymbol{\tau}}{\bar{\tau}} = \tfrac{3}{2}\gamma \frac{\boldsymbol{\tau}}{\bar{\tau}} = \gamma \boldsymbol{n}, \tag{2}$$

where Q is the process activation energy, R the gas constant, θ the absolute temperature, f the viscosity parameter and Y is the flow stress. In general, the viscososity parameter f and the exponent m are functions of temperature [6, 15], however, in this study they are assumed to be constants. The reduced stress $\boldsymbol{\tau}$ is defined as a differerence of the stress deviator $\mathbf{s}$ and the back stress $\boldsymbol{B}$ as $\boldsymbol{\tau} = \boldsymbol{s} - \frac{2}{3}\boldsymbol{B}$. The scalar $\bar{\tau}$ is the reduced equivalent stress $\bar{\tau} = (\frac{3}{2}\boldsymbol{\tau}{:}\boldsymbol{\tau})^{1/2}$. The following hardening rules are used [1, 5, 13, 18]

$$\begin{aligned} \dot{Y} &= H_1\gamma - (H_2\gamma + H_3)(Y - Y_0)^2, \\ \dot{\boldsymbol{B}} &= K_1 \dot{\boldsymbol{\epsilon}}^{\text{in}} - (K_2\gamma + K_3)\bar{B}\boldsymbol{B}, \end{aligned} \tag{3}$$

where $H_1, ..., H_3, K_1, ..., K_3$ and Y_0 are material parameters and $\bar{B} = \sqrt{\frac{2}{3}\boldsymbol{B} : \boldsymbol{B}}$.

Assuming linear isotropic thermoelasticity, the whole set of evolution equations comprises hardening evolution equations (3) and the elasticity equations

$$\dot{\boldsymbol{s}} = 2G(\dot{\boldsymbol{e}} - \dot{\boldsymbol{\epsilon}}^{\text{in}}) + \frac{\partial G}{\partial \theta}\frac{\dot{\theta}}{G}\,\boldsymbol{s}, \qquad \dot{\sigma}_{\text{m}} = \kappa\ \text{trace}\ (\dot{\boldsymbol{\epsilon}} - \dot{\boldsymbol{\epsilon}}^{\text{th}}) + \frac{\partial \kappa}{\partial \theta}\frac{\dot{\theta}}{\kappa}\,\sigma_{\text{m}}, \tag{4}$$

where $\dot{\boldsymbol{e}}$ is the deviatoric strain rate, $\dot{\boldsymbol{\epsilon}}^{\text{th}} = C\dot{\theta}\boldsymbol{I}$ the thermal strain rate, $\sigma_{\text{m}} = \frac{1}{3}\text{trace}\ (\boldsymbol{\sigma})$ the mean stress and parameters G, κ are the shear and bulk modulus, respectively. The linear coefficient of thermal expansion is denoted as C. All the material parameters $G, \kappa, C, Y_0, H_1, H_2, H_3,\ K_1, K_2, K_3, Q, f$ and m can depend on temperature.

Schreyer [18] used the generalized trapezoidal rule to solve the evolution equations (3). In the following, the Schreyer's algorithm, extended with isotropic hardening, is briefly described. Denoting $\boldsymbol{\tau} = \boldsymbol{s} - \frac{2}{3}\boldsymbol{B}$ the system (3)-(4) can be written in a form

$$\begin{aligned} \dot{\boldsymbol{\tau}} + \tilde{A}_{11}\boldsymbol{\tau} + \tilde{A}_{12}\boldsymbol{B} &= \dot{\boldsymbol{s}}^{\text{trial}}, \\ \dot{\boldsymbol{B}} + \tilde{A}_{21}\boldsymbol{\tau} + \tilde{A}_{22}\boldsymbol{B} &= 0, \\ \dot{Y} - H_1\gamma + (H_2\gamma + H_3)(Y - Y_0)^2 &= 0, \end{aligned} \tag{5}$$

where

$$\begin{aligned} \tilde{A}_{11} &= (3G + K_1)\frac{\gamma}{\bar{\tau}} - \frac{\partial G}{\partial \theta}\frac{\dot{\theta}}{G}, & \tilde{A}_{12} &= -\tfrac{2}{3}(K_2\gamma + K_3)\bar{B} + \frac{\partial G}{\partial \theta}\frac{\dot{\theta}}{G}, \\ \tilde{A}_{21} &= -K_1\frac{3\gamma}{2\bar{\tau}}, & \tilde{A}_{22} &= (K_2\gamma + K_3)\bar{B}, \end{aligned} \tag{6}$$

and the elastic trial stress rate is defined as $\dot{\boldsymbol{s}}^{\text{trial}} = 2G\dot{\boldsymbol{e}}^{\text{e}}$.

Applying the generalized trapezoidal rule

$$\begin{aligned} \boldsymbol{\tau}_{n+1} &= \boldsymbol{\tau}_n + \Delta t\big(\alpha\dot{\boldsymbol{\tau}}_{n+1} + (1-\alpha)\dot{\boldsymbol{\tau}}_n\big), \\ \boldsymbol{B}_{n+1} &= \boldsymbol{B}_n + \Delta t\big(\alpha\dot{\boldsymbol{B}}_{n+1} + (1-\alpha)\dot{\boldsymbol{B}}_n\big), \\ Y_{n+1} &= Y_n + \Delta t\big(\alpha\dot{Y}_{n+1} + (1-\alpha)\dot{Y}_n\big) \end{aligned} \tag{7}$$

to the system (5), the discrete evolution equations are

$$\begin{aligned} A_{11}\boldsymbol{\tau}_{n+1} + A_{12}\boldsymbol{B}_{n+1} &= \boldsymbol{R}_1, \\ A_{21}\boldsymbol{\tau}_{n+1} + A_{22}\boldsymbol{B}_{n+1} &= \boldsymbol{R}_2, \\ Y_{n+1} - \Delta t\alpha\left[H_1\gamma_{n+1} - (H_2\gamma_{n+1} + H_3)(Y_{n+1} - Y_0)^2\right] &= Y_n \\ &\quad + \Delta t(1-\alpha)\left[H_1\gamma_n - (H_2\gamma_n + H_3)(Y_n - Y_0)^2\right], \end{aligned} \tag{8}$$

where

$$\begin{aligned} \boldsymbol{R}_1 &= a_{11}\boldsymbol{\tau}_n + a_{12}\boldsymbol{B}_n + \alpha\Delta t\dot{\boldsymbol{s}}^{\text{trial}}_{n+1} + (1-\alpha)\Delta t\dot{\boldsymbol{s}}^{\text{trial}}_{n}, \\ \boldsymbol{R}_2 &= a_{21}\boldsymbol{\tau}_n + a_{22}\boldsymbol{B}_n \end{aligned} \tag{9}$$

and

$$\begin{aligned} A_{11} &= 1 + \alpha\Delta t\tilde{A}_{11,n+1}, & a_{11} &= 1 - (1-\alpha)\Delta t\tilde{A}_{11,n}, \\ A_{12} &= \alpha\Delta t\tilde{A}_{12,n+1}, & a_{12} &= -(1-\alpha)\Delta t\tilde{A}_{12,n}, \\ A_{21} &= \alpha\Delta t\tilde{A}_{21,n+1}, & a_{21} &= -(1-\alpha)\Delta t\tilde{A}_{21,n}, \\ A_{22} &= 1 + \alpha\Delta t\tilde{A}_{22,n+1}, & a_{22} &= 1 - (1-\alpha)\Delta t\tilde{A}_{22,n}. \end{aligned} \tag{10}$$

Depending on the α-parameter, some well known schemes are obtained: $\alpha = 0$ corresponds to the explicit Euler scheme, $\alpha = 1/2$ the trapezoidal rule and $\alpha = 1$ the implicit, backward Euler scheme. Only the trapezoidal rule is asymptotically second order accurate, however, it produces oscillations when the time-step size exceeds the critical time-step of the explicit Euler method Δt_{cr}. As shown numerically in [12, 18, 19], the backward Euler is the most versatile scheme in this family of methods. However, the equations are expressed in this general form to facilitate a possibility to switch from implicit Euler to the trapezoidal rule when the time-step is smaller than Δt_{cr}.

Following the formulation in [18, 19], solution of this nonlinear system can be performed involving only the scalar "invariants" $\bar{\tau}$ and $\bar{B}$ and, in the present formulation also the flow stress Y. The two first equations in (8) can be solved formally as

$$\begin{aligned} \boldsymbol{\tau}_{n+1} &= (A_{22}\boldsymbol{R}_1 - A_{12}\boldsymbol{R}_2)/D, \\ \boldsymbol{B}_{n+1} &= (A_{11}\boldsymbol{R}_2 - A_{21}\boldsymbol{R}_1)/D, \end{aligned} \tag{11}$$

where $D = A_{11}A_{22} - A_{12}A_{21}$. Squaring both sides of equations (11), the resulting nonlinear algebraic system for the unknowns $\bar{\tau}, \bar{B}$ and Y is thus

$$\begin{aligned} F_1 =& \bar{\tau}_{n+1}D - \sqrt{\tfrac{3}{2}f_1} = 0, \\ F_2 =& \bar{B}_{n+1}D - \sqrt{\tfrac{2}{3}f_2} = 0, \\ F_3 =& Y_{n+1} - Y_n - \Delta t\alpha\left[H_1\gamma_{n+1} - (H_2\gamma_{n+1} + H_3)(Y_{n+1} - Y_0)^2\right] \\ & - \Delta t(1-\alpha)\left[H_1\gamma_n - (H_2\gamma_n + H_3)(Y_n - Y_0)^2\right] = 0, \end{aligned} \tag{12}$$

where the following abbreviations are used

$$\begin{aligned} f_1 &= A_{22}^2 R_{11} - 2A_{22}A_{12}R_{12} + A_{12}^2 R_{22}, \\ f_2 &= A_{21}^2 R_{11} - 2A_{11}A_{21}R_{12} + A_{11}^2 R_{22}, \\ R_{ij} &= \boldsymbol{R}_i : \boldsymbol{R}_j. \end{aligned} \tag{13}$$

The formulas for A_{ij}, F_1 and F_2 differ slightly from those presented in [18] due to the difference in defining the direction of the inelastic deformation $\boldsymbol{n}$.

For this procedure, the algorithmic tangent stiffness matrix, which is necessary to obtain quadratic rate of convergence in the global equilibrium iterations, is given in the Appendix.

Selection of initial values

An important aspect in the Newton's iteration process of the system (12) is the selection of the initial values. Common choices utilize either the values from the previous converged step (i.e. variables at the beginning of the increment) or the stress increment is taken as elastic, while the internal variables have their values from previous converged step. An alternative approach is given by Schreyer [18, 19], where the steady state solution for the creep problem is used for the initial guess for the iteration. As shown numerically in the above cited references and also by the present authors, the steady state approach for the initial guess appears to be within the radius of convergence of the Newton-Raphson iteration. In many cases it is also more efficient than the conventional approaches.

The steady-state solution is obtained under the assumptions that $\dot{\boldsymbol{\tau}}$, $\dot{\boldsymbol{B}}$ and $\dot{Y}$ are zero and the elastic deviatoric trial stress $\dot{\boldsymbol{s}}^{\text{trial}}$ is constant. This is obtained if

$$\begin{aligned}
\dot{\boldsymbol{\epsilon}}^{\text{in}} &= \dot{\boldsymbol{e}}, \\
\gamma_{\text{ss}} &= \sqrt{\tfrac{2}{3}\dot{\boldsymbol{e}} : \dot{\boldsymbol{e}}}, \\
Y_{\text{ss}} &= \sqrt{H_1\gamma_{\text{ss}}/(H_2\gamma_{\text{ss}} + H_3)} + Y_0
\end{aligned} \tag{14}$$

and τ_{ss} can be solved from equation (3). The steady-state solution for the invariant of the initial backstress is

$$\bar{B}^2_{\text{ss}} = \frac{K_1\gamma_{\text{ss}}}{K_2\gamma_{\text{ss}} + K_3}. \tag{15}$$

In some cases, where the parameters K_2 and K_3 are small, the steady state solution for the initial backstress will be inaccurate, resulting inefficient iteration. To prevent such situations, the initial value for the steady state backstress can be safeguarded by comparing it to the elastic effective stress $\bar{\sigma}^{\text{el}}$. A modification strategy could thus be: if $\bar{B}_{\text{ss}} > \bar{\sigma}^{\text{el}}$, then the initial value for $\bar{B}$ is taken from the previous converged step.

Numerical studies

Selection of the initial values for the iterates is of primary importance when large steps are used in the analysis. Behaviour of different choices is tested in a realistic problem. A single solder bump of a ball grid array (BGA) is analyzed under a combined thermal and mechanical loading. For simplicity, the movement between the board and the component is approximated by prescribing the displacements in x and z directions on the upper surface of the bump, see Fig. 1. The FE mesh consists of 540 standard trilinear 8-noded hexahedral elements, integrated with $2 \times 2 \times 2$ Gaussian quadrature. Loading consists of spatially uniformly distributed and temporally sinusoidal temperature variation $\theta(t) = \theta_0 + \frac{1}{2}\Delta\theta \sin(2\pi t/t_{\text{max}})$, where $\theta_0 = 293$ K and $\Delta\theta = 100$ K, and prescribed displacements on the upper surface of the bump $(u, v, w) = (\delta, 0, \delta)\sin(2\pi t/t_{\text{max}})$ and $\delta = 0.1$ μm.

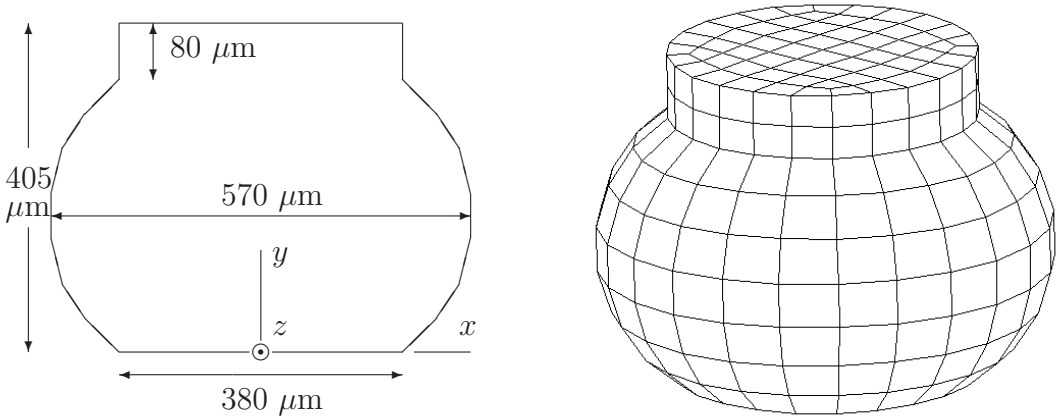

Figure 1. Solder bump; geometry and FE mesh [12, Fig. 12].

Table 1. Material parameters of the binary near eutectic Sn40Pb solder [1]. Parameters K_2 and K_3 are varied in the numerical tests and defined in (16).

E	=	33 GPa	Q	=	12 kcal/mol
ν	=	0.3	R	=	$2{\cdot}10^{-3}$ kcal/mol·K
Y_0	=	20 MPa	H_1	=	$E/165$
m	=	3.5	K_1	=	$E/100$
f	=	10^5 s^{-1}	C	=	$1.7\cdot10^{-5}$ K^{-1}

Material parameters are given in Table 1. Since the values of the non-linear kinematic hardening parameters K_2 and K_3 strongly affects on the initial value of the effective backstress, they are varied in a vide range. As defined in [18, 19] the nondimensional parameters ξ_2, ξ_3 are

$$K_2 = \xi_2 \frac{2G}{Y_0^2} \qquad K_3 = \xi_3 \frac{2G\gamma_0}{Y_0^2} \tag{16}$$

where $\gamma_0 = f\exp(-Q/R\theta)$. Using the data in Table 1, it gives the values $2G/Y_0^2 = 63.46$ mm/N and $2G\gamma_0/Y_0^2 = 8.1110^{-3}$ mm/Ns, evaluated at temperature $\theta = 293$ K. Since the non-linear isotropic hardening does not have much effect on the performance on solution algorithm, the parameters H_2 and H_3 are assumed to be zero. In addition, all material parameters in this test are assumed to be temperature independent.

Time interval $[0, t_{\max}]$ is divided into 12 equal timesteps. Four different choices for the initial values are tested: (i) initial state as the last converged state, marked as "init." in Table 2, (ii) state where the elastic predictor is added to the previous converged state, marked as "elast.", (iii) saturated values according to equations (14) and (15), and (iv) the modified strategy marked as "mod. satur.". The modified strategy is the safeguarded version of the steady state estimate, described in the previous section. Average numbers of Newton's iterations needed at the integration point level are recorded in Table 2.

Failure, as recorded in Table 2, is claimed when either the local Newton iteration at any integration point or the global Newton iteration does not converge within 20 corrector iterations. In a production code, failure at the integration point level might be avoided by using substepping. Continuation after a failure at the global equilibrium iteration level might be possible with a smaller time-step. The convergence for both iterations is tested

Table 2. Comparison of different choices for the initial iterate. The critical time step for the explicit Euler method is denoted as Δt_{cr}, and it is determined from the predictor state, see [12].

Δt	average $\Delta t/\Delta t_{\mathrm{cr}}$	max $\Delta t/\Delta t_{\mathrm{cr}}$	ξ_2	ξ_3	average number of iterations			
					init.	elast.	satur.	mod. satur.
50 s	1.8	13.0	0	0	5.5	6.1	4.3	4.3
			10^{-4}	10^{-4}	5.8	fail	4.7	4.3
			10^{-2}	10^{-2}	fail	fail	4.5	4.5
			1	1	fail	fail	4.7	4.7
			10	10	fail	fail	4.7	4.7
			10^2	10^2	fail	fail	fail	fail
500 s	4.0	23.6	0	0	5.5	7.5	4.0	4.0
			10^{-6}	10^{-6}	6.1	fail	4.5	4.0
			10^{-4}	10^{-4}	fail	fail	4.3	4.1
			10^{-2}	10^{-2}	fail	fail	4.3	4.3
			1	1	fail	fail	4.4	4.4
			10	10	fail	fail	4.5	4.5
			10^2	10^2	fail	fail	fail	fail
			10^2	0	fail	fail	4.5	4.5
			0	10^2	fail	fail	fail	fail

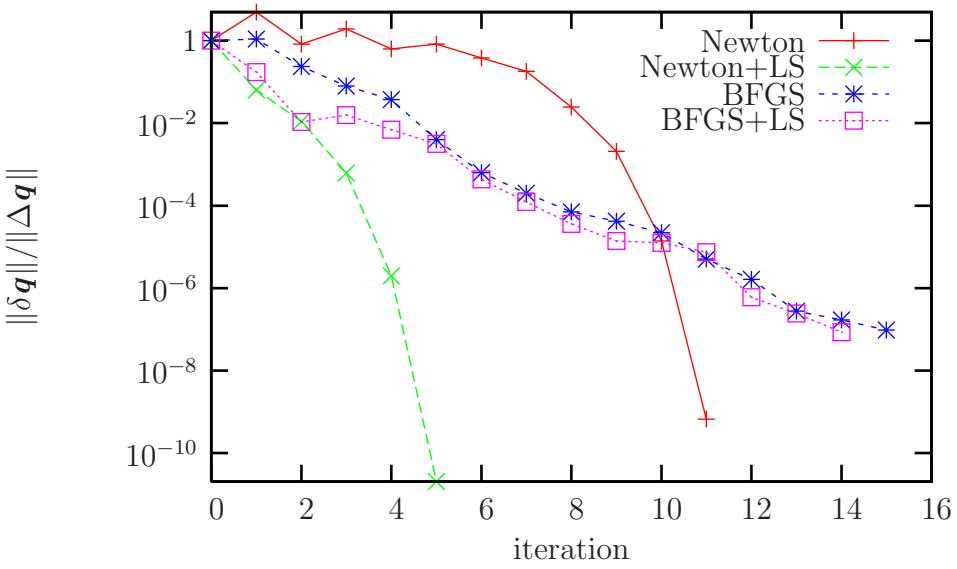

Figure 2. Equilibrium iteration history at the first step $\Delta t = 500$ s.

as $\|\boldsymbol{x}^{k+1} - \boldsymbol{x}^{k}\| < \varepsilon_{\mathrm{rel}}\|\boldsymbol{x}^{k+1} - \boldsymbol{x}^{0}\| + \varepsilon_{\mathrm{abs}}$, where the values $\varepsilon_{\mathrm{rel}} = 10^{-6}$ and $\varepsilon_{\mathrm{abs}} = 10^{-9}$ have been used and $\boldsymbol{x}$ is the displacement vector $\boldsymbol{q}$ in the global equilibrium iterations and $\boldsymbol{x} = (\bar{\tau}, \bar{B}, Y)^{\mathrm{T}}$ in the local iteration at the integration point level.

In Fig. 2 the global equilibrium iteration history is shown from the first step. It is clearly seen that only one line-seach will reduce the number of Newton's iterations from 11 to 5. For the Broyden-Fletcher-Goldfarb-Shanno (BFGS) quasi-newton iteration, application of the line-search does not give any improvement.

Concluding remarks

For standard elasto-plastic models the backward Euler method seems to be the best integration scheme [2, 9, 10, 11, 14, 17, 20, 21]. However, if there are other ingredients in the model, e.g. damage, other integration schemes could be more appropriate [22].

It is shown in many papers [12, 18, 19], that the backward Euler scheme seems to be unbeatable in creep computations – simple to code, accurate and relatively fast – especially when large time-steps are used. The key point in the success of the implicit Euler scheme is that the error in the computations using large, practically relevant timesteps is smaller than in other (even higher order) schemes. Many schemes having higher order asymptotic accuracy are inferior to the first order accurate implicit Euler scheme when the size of the time-step exceeds the critical time-step of the explicit Euler method, see [12, Fig. 2].

For analyses where large timesteps have to be used, the steady state solution for the initial guess, proposed by Schreyer, results in much larger convergence domain than the conventional approaches.

Appendix: Consistent algorithmic tangent

To obtain asymptotically quadratic convergence for the Newton iteration of the global equilibrium equations, the Jacobian of the discretized non-linear evolution equations of material model has to be evaluated. In the literature this Jacobian is often called the consistent algorithmic tangent, see e.g. [2, 16, 21]. It is defined as

$$\mathsf{C} = \frac{\partial \boldsymbol{\sigma}}{\partial \boldsymbol{\epsilon}} = \frac{\partial}{\partial \boldsymbol{\epsilon}} \left(\boldsymbol{s} + \sigma_{\mathrm{m}} \boldsymbol{I} \right) = \mathsf{C}_{\mathrm{dev}} + \mathsf{C}_{\mathrm{iso}} \tag{17}$$

and it is evaluated from quantities at the end of the current step at time t_{n+1}. In sequel, the subscript $n+1$ is omitted in places where there is no danger for confusion. Since the behaviour of the isotropic part of the stess is linear, thus $\mathsf{C}_{\mathrm{iso}} = \mathsf{C}^{\mathrm{el}}_{\mathrm{iso}}$. In the algorithm, the deviatoric stress is computed as

$$\boldsymbol{s} = \boldsymbol{\tau} + \tfrac{2}{3}\boldsymbol{B} = D^{-1} \left[\left(A_{22} - \tfrac{2}{3} A_{21} \right) \boldsymbol{R}_1 + \left(\tfrac{2}{3} A_{11} - A_{12} \right) \boldsymbol{R}_2 \right] \tag{18}$$

and using the following notations: $\partial \boldsymbol{R}_1 / \partial \boldsymbol{\epsilon} = \alpha \mathsf{C}^{\mathrm{el}}_{\mathrm{dev}}$ and $\partial \boldsymbol{R}_2 / \partial \boldsymbol{\epsilon} \equiv \mathsf{0}$ and $D = A_{11}A_{22} - A_{12}A_{21}$, the deviatoric part of the stiffness tensor can be expressed as

$$\begin{aligned} \frac{\partial \boldsymbol{s}}{\partial \boldsymbol{\epsilon}} = \frac{1}{D} \Bigg[& \left(\tfrac{2}{3}\boldsymbol{R}_2 - A_{22}\boldsymbol{s} \right) \frac{\partial A_{11}}{\partial \boldsymbol{\epsilon}} + \left(A_{21}\boldsymbol{s} - \boldsymbol{R}_2 \right) \frac{\partial A_{12}}{\partial \boldsymbol{\epsilon}} + \left(A_{12}\boldsymbol{s} - \tfrac{2}{3}\boldsymbol{R}_1 \right) \frac{\partial A_{12}}{\partial \boldsymbol{\epsilon}} \\ & + \left(\boldsymbol{R}_1 - A_{11}\boldsymbol{s} \right) \frac{\partial A_{22}}{\partial \boldsymbol{\epsilon}} + \alpha \left(A_{22} - \tfrac{2}{3} A_{21} \right) \mathsf{C}^{\mathrm{el}}_{\mathrm{dev}} \Bigg] \end{aligned} \tag{19}$$

Derivatives for the scalars A_{ij} are:

$$\begin{aligned}
\frac{\partial A_{11}}{\partial \boldsymbol{\epsilon}} &= \alpha\Delta t \frac{(3G+K_1)}{\bar{\tau}^2}\left(\bar{\tau}\frac{\partial \gamma}{\partial \boldsymbol{\epsilon}} - \gamma\frac{\partial \bar{\tau}}{\partial \boldsymbol{\epsilon}}\right)\\
\frac{\partial A_{12}}{\partial \boldsymbol{\epsilon}} &= -\frac{2}{3}\alpha\Delta t\left[(K_2\gamma + K_3)\frac{\partial \bar{B}}{\partial \boldsymbol{\epsilon}} + K_2\bar{B}\frac{\partial \gamma}{\partial \boldsymbol{\epsilon}}\right]\\
\frac{\partial A_{21}}{\partial \boldsymbol{\epsilon}} &= -\frac{3}{2}\alpha\Delta t\frac{K_1}{\bar{\tau}^2}\left(\bar{\tau}\frac{\partial \gamma}{\partial \boldsymbol{\epsilon}} - \gamma\frac{\partial \bar{\tau}}{\partial \boldsymbol{\epsilon}}\right)\\
\frac{\partial A_{22}}{\partial \boldsymbol{\epsilon}} &= \alpha\Delta t\left[(K_2\gamma + K_3)\frac{\partial \bar{B}}{\partial \boldsymbol{\epsilon}} + K_2\bar{B}\frac{\partial \gamma}{\partial \boldsymbol{\epsilon}}\right]
\end{aligned} \tag{20}$$

Derivative of the creep strain rate γ can be expressed as

$$\frac{\partial \gamma}{\partial \boldsymbol{\epsilon}} = \frac{\partial \gamma}{\partial \bar{\tau}}\left(\frac{\partial \bar{\tau}}{\partial \boldsymbol{\epsilon}} - \frac{\bar{\tau}}{Y}\frac{\partial Y}{\partial \boldsymbol{\epsilon}}\right) \tag{21}$$

where

$$\frac{\partial \gamma}{\partial \bar{\tau}} = C_F = \frac{mf}{Y}\exp\left(\frac{-Q}{R\theta}\right)\sinh^{m-1}\left(\frac{\bar{\tau}}{Y}\right)\cosh\left(\frac{\bar{\tau}}{Y}\right) \tag{22}$$

It can be seen that the derivative with respect to the flow stress can be written as $\partial Y/\partial \boldsymbol{\epsilon} = C_H \partial \bar{\tau}/\partial \boldsymbol{\epsilon}$, where the coefficient C_H depend on the chosen isotropic hardening model. For the model (3) it has the form

$$C_H = \frac{h_1}{1+h_2} \tag{23}$$

where

$$h_1 = C_F\frac{\alpha\Delta t[H_1 - H_2(Y-Y_0)^2]}{1+2\alpha\Delta t(H_2\gamma + H_3)(Y-Y_0)}, \qquad h_2 = h_1(\bar{\tau}/Y) \tag{24}$$

Derivatives (20) can be written as

$$\begin{aligned}
\frac{\partial A_{11}}{\partial \boldsymbol{\epsilon}} &= t_{11}\frac{\partial \bar{\tau}}{\partial \boldsymbol{\epsilon}} & \frac{\partial A_{12}}{\partial \boldsymbol{\epsilon}} &= t_{12}\frac{\partial \bar{\tau}}{\partial \boldsymbol{\epsilon}} + b_{12}\frac{\partial \bar{B}}{\partial \boldsymbol{\epsilon}}\\
\frac{\partial A_{21}}{\partial \boldsymbol{\epsilon}} &= t_{21}\frac{\partial \bar{\tau}}{\partial \boldsymbol{\epsilon}} & \frac{\partial A_{22}}{\partial \boldsymbol{\epsilon}} &= t_{22}\frac{\partial \bar{\tau}}{\partial \boldsymbol{\epsilon}} + b_{22}\frac{\partial \bar{B}}{\partial \boldsymbol{\epsilon}}
\end{aligned} \tag{25}$$

where

$$\begin{aligned}
t_{11} &= \alpha\Delta t(3G+K_1)(C_F/\bar{\tau} - C_F C_H/Y - \gamma/\bar{\tau}^2) & t_{12} &= -\tfrac{2}{3}\alpha\Delta t K_2\bar{B}C_F(1 - C_H\bar{\tau}/Y)\\
t_{21} &= -\tfrac{3}{2}\alpha\Delta t K_1(C_F/\bar{\tau} - C_F C_H/Y - \gamma/\bar{\tau}^2) & t_{22} &= \alpha\Delta t K_2\bar{B}C_F(1 - C_H\bar{\tau}/Y)\\
b_{12} &= -\tfrac{2}{3}\alpha\Delta t(K_2\gamma + K_3) & b_{22} &= \alpha\Delta t(K_2\gamma + K_3)
\end{aligned} \tag{26}$$

Derivatives of the equivalent stresses $\bar{\tau}$ and $\bar{B}$ has to be evaluated from their algorithmic expressions in equations (12): $\bar{\tau} = \sqrt{\frac{3}{2}f_1}/D$ and $\bar{B} = \sqrt{\frac{2}{3}f_2}/D$. After some simple algebra

$$\begin{aligned}
\frac{\partial \bar{\tau}}{\partial \boldsymbol{\epsilon}} &= \boldsymbol{t}_0 + t_1\frac{\partial A_{11}}{\partial \boldsymbol{\epsilon}} + t_2\frac{\partial A_{12}}{\partial \boldsymbol{\epsilon}} + t_3\frac{\partial A_{21}}{\partial \boldsymbol{\epsilon}} + t_4\frac{\partial A_{22}}{\partial \boldsymbol{\epsilon}}\\
\frac{\partial \bar{B}}{\partial \boldsymbol{\epsilon}} &= \boldsymbol{b}_0 + b_1\frac{\partial A_{11}}{\partial \boldsymbol{\epsilon}} + b_2\frac{\partial A_{12}}{\partial \boldsymbol{\epsilon}} + b_3\frac{\partial A_{21}}{\partial \boldsymbol{\epsilon}} + b_4\frac{\partial A_{22}}{\partial \boldsymbol{\epsilon}}
\end{aligned} \tag{27}$$

where

$$\boldsymbol{t}_0 = \frac{3\alpha}{2D^2\bar{\tau}}\left(A_{22}^2\mathsf{C}_{\mathrm{dev}}^{\mathrm{el}}\colon \boldsymbol{R}_1 - A_{12}A_{22}\mathsf{C}_{\mathrm{dev}}^{\mathrm{el}}\colon \boldsymbol{R}_2\right) \qquad \boldsymbol{b}_0 = \frac{2\alpha}{3D^2\bar{B}}\left(A_{21}^2\mathsf{C}_{\mathrm{dev}}^{\mathrm{el}}\colon \boldsymbol{R}_1 - A_{21}A_{11}\mathsf{C}_{\mathrm{dev}}^{\mathrm{el}}\colon \boldsymbol{R}_2\right)$$

$$t_1 = -\bar{\tau}D^{-1}A_{22} \qquad b_1 = \frac{2}{3D^2\bar{B}}\left(A_{11}R_{22} - A_{21}R_{12}\right) - \bar{B}D^{-1}A_{22}$$

$$t_2 = \frac{3}{2D^2\bar{\tau}}\left(A_{12}R_{22} - A_{22}R_{12}\right) + \bar{\tau}D^{-1}A_{21} \qquad b_2 = \bar{B}D^{-1}A_{21}$$

$$t_3 = \bar{\tau}D^{-1}A_{12} \qquad b_3 = \frac{2}{3D^2\bar{B}}\left(A_{21}R_{11} - A_{11}R_{12}\right) + \bar{B}D^{-1}A_{12}$$

$$t_4 = \frac{3}{2D^2\bar{\tau}}\left(A_{22}R_{11} - A_{12}R_{12}\right) - \bar{\tau}D^{-1}A_{11} \qquad b_4 = -\bar{B}D^{-1}A_{11} \tag{28}$$

Substituting expressions (20) into the equations (27), derivatives $\boldsymbol{t}_\epsilon = \partial\bar{\tau}/\partial\boldsymbol{\epsilon}$ and $\boldsymbol{b}_\epsilon = \partial\bar{B}/\partial\boldsymbol{\epsilon}$ can be solved from the equation

$$\begin{aligned} T_{11}\boldsymbol{t}_\epsilon - T_{12}\boldsymbol{b}_\epsilon &= \boldsymbol{t}_0 \\ -T_{21}\boldsymbol{t}_\epsilon + T_{22}\boldsymbol{b}_\epsilon &= \boldsymbol{b}_0 \end{aligned} \tag{29}$$

where

$$\begin{aligned} T_{11} &= 1 - t_1t_{11} - t_2t_{12} - t_3t_{21} - t_4t_{22} \\ T_{12} &= t_2b_{12} + t_4b_{22} \\ T_{21} &= b_1t_{11} + b_2t_{12} + b_3t_{21} + b_4t_{22} \\ T_{22} &= 1 - b_2b_{12} - b_4b_{22} \end{aligned} \tag{30}$$

Finally, the deviatoric part of the consistent algorithmic tangent tensor can be written in the form

$$\mathsf{C}_{\mathrm{dev}} = \frac{1}{D}\left[\alpha\left(A_{22} - \tfrac{2}{3}A_{21}\right)\mathsf{C}_{\mathrm{dev}}^{\mathrm{el}} + \boldsymbol{e}_1\boldsymbol{t}_\epsilon + \boldsymbol{e}_2\boldsymbol{b}_\epsilon\right] \tag{31}$$

where the second order tensors $\boldsymbol{e}_1$ and $\boldsymbol{e}_2$ are

$$\begin{aligned} \boldsymbol{e}_1 &= \left[-\left(A_{22} - \tfrac{2}{3}A_{21}\right)t_{11} + \left(A_{12} - \tfrac{2}{3}A_{11}\right)t_{21}\right]\boldsymbol{\tau} - \left[\left(A_{22} - \tfrac{2}{3}A_{21}\right)t_{12} - \left(A_{12} - \tfrac{2}{3}A_{11}\right)t_{22}\right]\boldsymbol{B} \\ \boldsymbol{e}_2 &= \left[\left(A_{12} - \tfrac{2}{3}A_{11}\right)b_{22} - \left(A_{22} - \tfrac{2}{3}A_{21}\right)b_{12}\right]\boldsymbol{B} \end{aligned} \tag{32}$$

The algorithmic tangent is symmetric, although it is rather hard to see this directly in (31). It should be noticed, that tensors $\boldsymbol{t}_\epsilon$ and $\boldsymbol{b}_\epsilon$ are functions of $\boldsymbol{R}_1$ and $\boldsymbol{R}_2$ which are defined in (9) by quantities evaluated at time t_n, but which can also be expressed as in equations (8) with quantities evaluated at time t_{n+1}.

The derivations above are valid when the generalized trapezoidal rule is used to integrate the constitutive model in question. If the discontinuos Galerkin method with piecewise constant trial functions is used [4], terms A_{ij} in equations (10) should be replaced with those defined in equations (52) in [12] and expressions (26) and (24) are

changed to:

$$
\begin{aligned}
t_{11} &= \int_{t_n}^{t_{n+1}} (3G + K_1)(C_F/\bar{\tau} - C_F C_H/Y - \gamma/\bar{\tau}^2)\ \mathrm{d}t \\
t_{12} &= -\tfrac{2}{3} \int_{t_n}^{t_{n+1}} K_2 \bar{B} C_F (1 - C_H \bar{\tau}/Y)\ \mathrm{d}t \\
t_{21} &= -\tfrac{3}{2} \int_{t_n}^{t_{n+1}} K_1 (C_F/\bar{\tau} - C_F C_H/Y - \gamma/\bar{\tau}^2)\ \mathrm{d}t \\
t_{22} &= \int_{t_n}^{t_{n+1}} K_2 \bar{B} C_F (1 - C_H \bar{\tau}/Y)\ \mathrm{d}t \\
b_{12} &= -\tfrac{2}{3} \int_{t_n}^{t_{n+1}} (K_2 \gamma + K_3)\ \mathrm{d}t \\
b_{22} &= \int_{t_n}^{t_{n+1}} (K_2 \gamma + K_3)\ \mathrm{d}t
\end{aligned}
\tag{33}
$$

$$
\begin{aligned}
h_1 &= \int_{t_n}^{t_{n+1}} C_F \left[H_1 - H_2 (Y_{n+1} - Y_0)^2 \right]\ \mathrm{d}t \\
h_2 &= 2A_{33}(Y_{n+1} - Y_0) + \int_{t_n}^{t_{n+1}} C_F \left[H_1 - H_2 (Y_{n+1} - Y_0)^2 \right] (\bar{\tau}/Y)\ \mathrm{d}t
\end{aligned}
\tag{34}
$$

References

[1] S.N. Burchett, M.K. Neilsen, D.R. Frear, J.J. Stephens. Computational continuum modelling of solder interconnects. In R.K. Mahidhara et al., editors, *Design and Reliability of Solders and Solder Interconnects*, pages 171–178, The Minerals, Metals & Materials Society, (1997).

[2] J.L. Chaboche, G. Cailletaud. Integration methods for complex plastic constitutive equations. *Computer Methods in Applied Mechanics and Engineering*. 1996, **133**, 125–155.

[3] N.A. Cyr, R.D. Teter. Finite element elastic-plastic-creep analysis of two-dimensional continuum with temperature dependent material properties *Computers & Structures*. 1973, **3**, 849–863.

[4] K. Eriksson, D. Estep, P. Hansbo, C. Johnsson. *Computational Differential Equations*. Studentlitteratur, 1996.

[5] D.R. Frear, S.N. Burchett, M.K. Neilsen, J.J. Stephens. Microstructurally based finite element simulation of solder joint behaviour. *Soldering & Surface Mount Technology*. 1997, **1** (25), 39–42.

[6] F. Garofalo. *Fundamentals of Creep and Creep-Rupture in Metals*. The MacMillan Co.: New York, 1965.

[7] T.J.R. Hughes, R.L. Taylor. Unconditionally stable algorithms for quasi-static elasto/visco-plastic finite element analysis. *Computers & Structures*. 1978, **8**, 169–173.

[8] M.B. Kanchi, O.C. Zienkiewicz, D.R.J. Owen. The visco-plastic approach to problems of plasticity and creep involving geometric non-linear effects. *International Journal for Numerical Methods in Engineering* 1978, **12**, 169–181.

[9] R.D. Krieg and D.B. Krieg. Accuracies of numerical solution methods for the elastic-perfectly plastic model *J. Pressure Vessel Technology*, 1977 **101**, 510–515.

[10] E. Kirchner, F.G. Kollmann. Application of modern time integrators to Hart's inelastic model. *International Journal of Plasticity*. 1999, **15**, 647–666.

[11] E. Kirchner, B. Simeon. A higher-order time integration method for viscoplasticity. *Computer Methods in Applied Mechanics and Engineering* 1999, **175**, 1–18.

[12] R. Kouhia, P. Marjamäki, J. Kivilahti. On the integration of rate-dependent inelastic constitutive models, *International Journal for Numerical Methods in Engineering* 2005, **62**, 1832-1856.

[13] A. Miller. An inelastic constitutive model for monotonic, cyclic and creep deformations: Part I – equations development and analytical procedures. *Journal of Engineering Materials Technology* 1976, **98**, 97–105.

[14] Q.S. Nguyen. On the elasto-plastic initial boundary value problem and its numerical integration *International Journal for Numerical Methods in Engineering* 1977, **11**, 817–832.

[15] H. Riedel. *Fracture at High Temperature*. MRE Materials Research and Engineering. Springer-Verlag, Berlin, Heidelberg, 1987.

[16] M. Ristinmaa. Consistent stiffness matrix in fe calculations of elasto-plastic bodies. *Computers & Structures*. 1994, **50**, 93–103.

[17] K. Runesson, S. Sture, K. Willam. Integration in computational plasticity. *Computers & Structures*. 1988, **30** (1/2), 119–130.

[18] H.L. Schreyer. Unconditionally stable time integration of creep constitutive equations. Eccomas 2000, Barcelona 11-14 September 2000, CD-ROM Proceedings.

[19] H.L. Schreyer. On time integration of viscoplastic constitutive models suitable for creep. *International Journal for Numerical Methods in Engineering* 2002, **53** (3), 637–652.

[20] H.L. Schreyer, R.F. Kulak, J.M. Kramer. Accurate numerical solutions for elastic-plastic models. *J. Pressure Vessel Technology*, 1979, **101**, 226–234.

[21] J.C. Simo and T.J.R. Hughes. *Computational Inelasticity*. Springer: New York, 1998.

[22] M. Wallin, M. Ristinmaa. Accurate stress updating algorithm based on constant strain rate assumption. *Computer Methods in Applied Mechanics and Engineering* 2001, **190** (42), 5583–5601.

[23] P.J. Yoder, R.L. Whirley. On the numerical implementation of elastoplastic models. *Journal of Applied Mechanics* 1984, **51**, 283–287.

Reijo Kouhia
Department of Mechanical Engineering and Industrial Systems
Tampere University of Technology
P.O. Box 589, FI-33101 Tampere, Finland
reijo.kouhia@tut.fi

Pekka Marjamäki
Pöyry Finland Oy
Jaakonkatu 3, FI-01650 Vantaa, Finland
pekka.marjamaki@poyry.com

Jorma Kivilahti
Department of Electronics
Aalto University
jkkivilahti@gmail.com